This is author version of article published as:

Miao, Xigeng and Sun, Dandan and Hoo, Pui Woon (2007) Effect of Y-TZP addition on the microstructure and properties of titania-based composites. *Ceramics International*.

Effect of Y-TZP addition on the microstructure and properties of titania-based composites

Xigeng Miao[1]*, Dandan Sun[1], Pui Woon Hoo[2]

[1]Institute of Health and Biomedical Innovation and School of Engineering Systems, Queensland University of Technology, Kelvin Grove, QLD 4059, Australia.

[2]School of Materials Science and Engineering, Nanyang Technological University, Nanyang Avenue, 639798, Singapore.

* Corresponding author. Tel: +61-7-3138-6237 fax: +61-7-3138-1516
E-mail: x.miao@qut.edu.au (X. Miao).

Abstract

To maintain the bioactivity and improve the mechanical properties of titania, both pure titania ceramics and titania-yttria-stabilized tetragonal zirconia (Y-TZP) composites with 5, 10, and 15 vol% Y-TZP were prepared via a sol-gel precipitation method. A titania precursor (titanium butoxide) was mixed with a submicron-sized Y-TZP powder, followed by hydrolysis-condensation reactions, green compact forming, and sintering in air at 1200^{o}C to 1350^{o}C. It was found that the addition of Y-TZP resulted in reduced rutile titania grain size from 13 μm to 3 μm. The Y-TZP tetragonal phase also resulted in improved mechanical properties of the titania-Y-TZP composites. For instance, the titania-15vol%Y-TZP composite had a hardness value of 983 kg/mm^2, a bending strength of 160 MPa, and a fracture toughness of 3.79 MPa.m$^{0.5}$. While the addition of Y-TZP increased the mechanical properties, it also decreased the bioactivity of the composites.

Keywords: A. Titania; B. Zirconia; C. Mechanical properties; D. Bioactivity

1. Introduction

Titania (TiO_2) ceramics have two polymorphs, namely, anatase phase and rutile phase and are traditionally used for catalysts, pigments, etc. However, titania ceramics have recently been studied as potential biomaterials. This emerging research interest could be triggered by the bone bonding ability of titania. Keshmiri *et al.* [1] showed that titania microspheres in the anatase phase were able to induce apatite formation after immersion in the simulated body fluid. Similarly, titania films of the anatase phase were found to be bioactive, judged by the formation of an apatite layer in vitro [2, 3]. The bioactivity of rutile titania was confirmed in

vitro [4]. Animal implantation tests also showed that titania ceramics even in the rutile phase could bond directly to bone [5]. Compared with the well known bioactive hydroxyapatite and bioglass, which show relatively faster dissolution in vivo, titania ceramics are relatively stable in vivo and the bonding between bone tissues and titania implants could be maintained for a long period of time [5]. Titania could also bond to a soft tissue [6], which is desirable for dental implant applications.

In spite of the desirable bioactivity of titania ceramics, pure titania ceramic monoliths are rarely used due to the tendency of large grain growth and the low mechanical properties. Titania has been mostly used in the form of coatings on strong substrates or implants [3]. Some titania/ polymer composites have also been found in the literature [7]. Specifically, for titania-based ceramic composites, Oh et al. [8] produced dense TiO_2 ceramics with TiO_2-TCP composite surfaces by a conventional sintering method. Li et al. [9] produced TiO_2-HA (hydroxyapatite) composites by hot isostatic pressing. However, the above studies were mainly for improving the biological behavior, rather than the mechanical properties of the titania. Very recently, Hanada et al. [10] used the spark plasma sintering technique to produce titania-based composites with dispersed diamond nanoparticles for biomedical applications.

Yttria-stabilized zirconia (Y-TZP)–TiO_2 composites were attempted in our previous study [11], but it was limited to the high zirconia contents and had the problem of the formation of zirconium titanate compound (thus depleting the anatase/rutile phases) due to the high sintering temperatures used. The purpose of the present study was to add Y-TZP second phase into titania matrices to form titania-Y-TZP composites, which would exhibit bioactivity due to the retention of anatase/ rutile titania phases and possess better mechanical properties due to the tetragonal to monoclinic phase transformation toughening mechanism associated with Y-TZP [12]. To obtain the titania-Y-TZP composites with the desirable phases, the sintering temperatures and the Y-TZP contents were designed based on the results of our previous study on Y-TZP (major)–titania (minor) composites [11]. This paper specifically reports the effect of Y-TZP addition (0-15 vol% Y-TZP) on the structural development, mechanical properties, and bioactivity of the titania-Y-TZP composites sintered at 1200 ^{o}C to 1350 ^{o}C.

2. Experimental procedure

2.1. Preparation

Titania powder was produced from titanium butoxide ($Ti(OC_4H_9)_4$) precursor (Aldrich Chemical Company, Inc.) in ambient conditions, in a similar way to the method reported by Ding et al. [13]. The precursor $Ti(OC_4H_9)_4$ was first added to ethanol at a volume ratio of 1:5. This solution was stirred rigorously while distilled water was added into it drop-wise. The Ti^{4+} to H_2O molar ratio was fixed at 1:100. To ensure complete hydrolysis and homogenous mixing, the colloidal suspension (sol) was stirred for extra 30 minutes after adding the last drop of water. Then, the sol was heated to evaporate the ethanol and water. The gel formed from the sol was further dried at 70°C overnight and the dried gel was crushed into powders.

The same Ti^{4+} to ethanol and Ti^{4+} to H_2O ratios were used in the synthesis of titania-yttria-stabilised tetragonal zirconia polycrystal (Y-TZP) colloidal mixtures, with 5, 10, and 15vol% Y-TZP. Commercially available Y-TZP (ZrO_2 (3-mol%Y_2O_3), Aldrich Chemical Company, Inc.) powder with sub-micron particle size, was ball-milled for 60 minutes at 150rpm in ethanol to break the agglomerates, resulting in a colloidal dispersion of 20wt% Y-TZP in

ethanol. The titania-Y-TZP colloidal mixtures were obtained by adding Y-TZP colloidal suspension together with distilled water drop-wise into the titanium butoxide dissolved in ethanol, so that the Y-TZP particles were dispersed into the titanium hydroxide precipitates. The colloidal mixtures were further stirred, heated and dried in the same way as for preparing pure titania powder.

Finally, pure titania powder and titania-Y-TZP mixed powders were uniaxially pressed into pellets of different sizes and shapes under the pressure of 200 MPa. They were then sintered at 1200°C, 1250°C, 1300°C and 1350°C in air for 4 hours at the heating and cooling rates of 5°C/min, respectively. Some sintered samples were ground, polished, and thermally etched for 30 minutes at 50°C below their respective sintering temperatures to reveal the grains. Furthermore, a polished titania-15vol%Y-TZP composite was used to perform a chemical treatment (etching) with a 5M hydrochloric acid (HCl) solution at 95°C for 4 days. The chemically treated samples were then washed with distilled water and dried in air. For the test of bioactivity, samples (treated and untreated) were immersed separately in a simulated body fluid (SBF based on Kokubo's recipe) and kept in an oven at a temperature of 37ºC for different durations up to several weeks. Then the immersed samples were rinsed with distilled water and dried to observe the formation of apatite surface layer.

2.2. Characterization

Thermogravimetry (TG) and differential thermal analysis (DTA) were performed on powder samples in oxygen atmosphere in a simultaneous TG/DTA analyser (NETZSCH STA 449C), at a heating rate of 10°C/min up to 1000°C. The thermal behavior of the green compacts was monitored by a dilatometer (NETSCH DIL 402C) with a heating rate of 5°C/min up to 1500°C. Fourier transform infra red (FTIR) spectra were recorded in the range of 4000 to 400cm^{-1} by using Perkin Elmer System 2000 FTIR spectrometer. The samples for FTIR were made from powder mixtures containing 80-85 wt.% dispersed KBr.

Phase analysis of the synthesised powders and the sintered samples was carried out using x-ray diffraction (XRD, Rigaku) with the Cu-K_α radiation. Thin film x-ray diffraction (TH-XRD) was also used for the analysis of surface phases. The elements on the surfaces of the chemically treated and untreated samples were characterised by x-ray photoelectron spectroscopy (XPS). The microstructural characteristics of powders ad sintered samples were observed under a scanning electron microscope (SEM, JEOL JSM-6360). The grain sizes were then estimated by the linear intercept method.

The bulk densities of the samples were measured by an electronic densimeter (Mirage MD-200S) based on the Achimedes principle. The relative density was taken as bulk density/ theoretical density, where the theoretical density of a composite was calculated by the rule of mixture. The Vickers hardness and the fracture toughness of the composites were measured using a microhardness tester (HSV-20, SHIDMAZU). In particular, the fracture toughness values were calculated using the equation given by Evans and Charles [14] and the Young's moduli of the composites were estimated by the rule of mixture. Finally, the flexural strengths of the samples were obtained by three-point-bending tests, carried out according to the ASTM Standard C1161.

3. Results and discussion

3.1. Initial powder state

Fig. 1 shows an SEM micrograph of the titania-10vol% Y-TZP mixed powder. The sub-micron sized Y-TZP particles (small) were dispersed among the large spherical titania particles (~1 μm in size). The as-synthesised pure titania (without calcination) was amorphous, whereas the Y-TZP particles in the mixed powders were in tetragonal phase. FTIR results showed the existence of Ti-OH groups in the titania particles. Thus, the so-called titania at this stage was actually $Ti(OH)_4$ rather than TiO_2. The formation of $Ti(OH)_4$ took place via the hydrolysis-condensation reaction between titanium butoxide and water in an ethanol solution, as shown in the following:

$$Ti(OC_4H_9)_4 + 4H_2O \rightarrow Ti(OH)_4 + 4C_4H_9OH \quad (6)$$

3.2. Thermal analysis in the heating process

For pure titania powders, TG analysis (i.e. weight loss) indicated that between 150°C to 400°C (Fig. 2), dehydroxylation of titanium hydroxide into titania occurred, i.e.

$$Ti(OH)_4 \rightarrow TiO_2 + H_2O \quad (7)$$

DTA analysis with additional XRD analysis indicated the occurrence of anatase phase of titania around 400°C. Thus, the dehydroxylation was immediately followed by crystallisation of anatase phase. The dehydrxylation and the formation of anatase phase also occurred in the in the titania-Y-TZP mixed powders. Furthermore, the addition of Y-TZP powder into titania did not alter the thermal behavior of titania significantly. The DTA analysis also indicated the transformation of the anatase phase to the rutile phase at above 600 ^oC.

3.3. Sintering behaviour in the heating process

Testing using the dilatometer indicated that all samples started to shrink at almost the same temperature of around 500°C. Furthermore, for pure titania, a major densification process occurred from 500°C to 850°C, whereas for the composites, another distinctive densification process took place in the temperature range of 1110°C to 1400°C. The temperature range of from 800°C to 1110°C in the sintering shrinkage-temperature curves was associated with a plateau only for the composites.

The sintering shrinkage rates (i.e. d(dL/L)/dT values) of pure titania and titania-Y-TZP composites are shown in Fig. 3. The temperature range with the fastest densification rate for pure titania corresponded to the densification of the fine anatase titania particles. The addition of the Y-TZP second phase led to different sintering behaviour of the composites compared to the pure titania. The sintering shrinkage rates of the composites with 10 vol% Y-TZP and 15 vol% Y-TZP in the temperature range from 500°C to 850°C (corresponding to the dominant densification of the anatase titania particles) were significantly smaller in absolute value than those of the pure titania and the composite with 5 vol% Y-TZP. This phenomenon could be due to the fact the Y-TZP second phase tended to impede the movement of the titania grain boundaries. In the temperature range of from 1100°C to 1400°C, the Y-TZP particles on their own became sinterable, due to the enhanced diffusion of elements and the relatively fine Y-TZP particle size.

3.4. Microstructure controlled by Y-TZP content and sintering temperature

XRD patterns of pure titania and titania-Y-TZP composites sintered at different temperatures (up to 1350^{o}C) for 4 hours were obtained. Titania in all the compositions was in anatase phase at 400 ^{o}C and it changed into rutile phase at temperatures higher than 600^{o}C, whereas Y-TZP in all the compositions was in the tetragonal phase. In the selected sintering temperature range from 1200^{o}C to 1350^{o}C, the titania-Y-TZP composites consisted of only

rutite phase and tetragonal zirconia phase. As shown in Fig. 4, with the increase of the Y-TZP content, the peaks ascribable to the tetragonal zirconia became more pronounced.

The densification of the titania ceramics and the titania-Y-TZP composites could be observed by examining the SEM images. In Fig. 5, one can see that pure titania was nearly fully densified at 1200 ^{o}C as few micropores were left in the ceramic sample. On the other hand, one can see a large number of micropores in the titania-15vol% Y-TZP composite. The zirconia particles were also well dispersed among the titania matrix. Obviously the addition of Y-TZP particles retarded the densification of the titania matrix. When the sintering temperature was inceased to 1350^{o}C, significantly different microstructures were obtained; as shown in Fig. 6, the titania grains grew significantly (up to ~12 μm in size) for the pure titania. On the other hand, the titania grains in the composite were relatively small (~3 μm) and the composite could be highly densified at the sintering temperature of 1350 ^{o}C.

Fig. 7 summarizes the relative densities as functions of the Y-TZP content and the sintering temperature. Obviously, the Y-TZP second phase reduced the densification. Only at 1350^{o}C, highly dense rutile titania-tetragonal zirconia composites could be obtained. It should be mentioned that temperatures higher than 1350 ^{o}C would result in the formation of zirconium titanate, which was undesirable for the present purpose. Fig. 8 shows the effect of sintering temperature and Y-TZP content on the titania grain growth. Obviously, the Y-TZP second phase tended to reduce the titania grain growth, especially at the sintering temperature of 1350^{o}C. The grain growth of titania phase was significant in the temperature range from 1300^{o}C to 1350^{o}C.

3.5. Mechanical properties

Fig. 9 shows the hardness values as a function of Y-TZP content for the titania-Y-TZP combinations sintered at various temperatures. The general trend was that Y-TZP addition significantly reduced the hardness for sintering temperatures of 1200^{o}C and 1300^{o}C. However, for the sintering temperature of 1350 ^{o}C, the hardness of the titania-15vol% composite was higher than that of the titania-10vol% Y-TZP composite. The decrease of the hardness with the addition of Y-TZP for the sintering temperatures of 1200^{o}C and 1300^{o}C was due to the poor densification of the composites, i.e., a high porosity resulted in a low hardness value. On the other hand, since dense Y-TZP ceramics normally have higher hardness than titania ceramics, thus dense titania-YTZP composites should have higher hardness than pure titania. The variation of hardness versus Y-TZP content for the 1350^{o}C sintering temperature could be due to the combined effects of the porosity and the intrinsic higher hardness of Y-TZP. In other words, the small amount of remaining porosity was responsible for the decrease of hardness. However, when the Y-TZP content was high enough, i.e., at 15vol%, the Y-TZP grains tended to form an interconnected network in the composite, which could contribute to the increase of the hardness.

Fig. 10 shows the increase of bending strength with the Y-TZP addition when the composites were sintered at 1350^{o}C and therefore had high relative densities (> 95%). As a fracture strength is sensitive to microstructure, the current favorable effect of Y-TZP on the strength could be explained by the reduced titania grain size and the high intrinsic strength of Y-TZP. For ceramic materials, large grain size means large residual thermal stresses due to the anisotropic thermal expansion coefficients of the individual grains. The addition of Y-TZP tended to reduce the titania grain size and thus reduce the thermal stresses. However, the addition of Y-TZP also introduced other thermal stresses originating from the thermal expansion coefficient mismatch between the two different phases (titania: ~7×10^{-6} °C^{-1}; Y-

TZP: ~10×10^{-6} $°C^{-1}$). Thus, the high densities achieved in the composites and the high intrinsic strength of Y-TZP could play important roles on the strength improvement.

The plot of the fracture toughness of titania-Y-TZP composites sintered at 1350°C versus Y-TZP content is shown in Fig. 11. The fracture toughness obviously increased with the Y-TZP addition. Note that the fracture toughness of pure titania was not available because abnormal cracks were developed around the peripheral of a Vickers indentation impression, which made the indentation method invalid. The abnormal cracking was related to the large titania grains and the residual thermal stresses.

The increased fracture toughness of the titania-Y-TZP composites could be due to the toughening mechanisms of (a) tetragonal to monoclinic zirconia phase transformation and (b) crack deflection due to the increased contribution of phase or grain boundaries. For instance, the transformation of tetragonal Y-TZP phase into the monoclinic phase would take place near the tip of a propagating crack when an external load was applied on the composite. The stress field resulting from the phase transformation at the tip counteracted the stress field caused by the externally applied load. In other words, the energy input for the crack to propagate was dissipated by the tetragonal to monoclinic phase transformation, and thus the toughness (or cracking resistance) of the composite increased.

3.6. Bioactivity

The pure titania ceramics showed apatite formation on their polished surfaces when they were immersed in the SBF for 20 days (Table 1). However, no apatite formation was found on the polished surface of the titania-15vol% Y-TZP composite even after 30 days of immersion. Thus one can see that titania had a low degree of bioactivity (related to the speed of apatite formation) as compared to bioactive glasses, which normally show apatite formation in a few days. The addition of Y-TZP obviously reduced the bioactivity of titania. Since apatite formation on a surface is a process of nucleation and grain growth, the surface conditions such as composition, crystal structure, and morphology have important effects on the apatite formation. Thus one can modify the surface conditions to improve the bioactivity. A surface can be modified by several ways such as coating, grinding, chemical etching [15], radiation [16], etc. In the present study, polishing and chemical treatment with 5M HCl was used to enhance the bioactivity of the titania-15vol% Y-TZP composite. In fact, islands of apatite crystals were observed on the treated composite surface after 20 days of immersion in the SBF and a continuous apatite layer was formed after 30 days of immersion in the SBF (Fig. 12). Similar observation was found in a relevant study [17], where the bioactivity of plasma sprayed titania coatings was improved by the acid treatment with H_2SO_4 and HCl solutions.

Recent studies showed that zirconia coatings with either tetragonal or monoclinic phase could also be bioactive [18]. Evan Zr metal could become bioactive after chemical treatment with NaOH [19]. Some zirconia composites that can be conventionally regarded as bioinert were also made bioactive after different surface treatments [16]. It should be mentioned that the leaching of yttrium ions away from Y-TZP by HCl was not ideal as Y-TZP phase should be stabilized by ytrria. Thus, in the future, NaOH solution should be used as Uchida et al. [20] could make Ce-TZP/Al_2O_3 nanocomposite bioactive. Thus, the bioactivity of titania-Y-TZP composites prepared in the present study seemed not surprising. The key for the bioactivity lies in the availability of Zr-OH and / or Ti-OH groups attached onto the sample surface. The functional groups were indeed confirmed by additional XPS study.

4. Conclusions

Titania-Y-TZP composites with 5, 10, 15 vol% of Y-TZP contents were produced by sintering at temperatures from 1200°C to 1350°C. The titania was present in the rutile phase, whereas the Y-TZP phase was in the tetragonal form of zirconia. The titania grain size was reduced from 12.8μm in the pure titania to 3.1μm in the titania-15vol%Y-TZP composite. The well-dispersed Y-TZP phase in the titania matrices and the reduced grain size of the titania matrices together contributed to the increased hardness, bending strength, and fracture toughness. In particular, the titania-15vol%Y-TZP composite sintered at 1350°C exhibited a hardness value of 983 kg/mm^2, a bending strength of 160 MPa, and a fracture toughness of 3.79 MPa.m$^{0.5}$, respectively. While the addition of Y-TZP increased the mechanical properties, it also decreased the bioactivity of the composites. However, the low degree of bioactivity of the relatively stable titania–Y-TZP composites could be advantageous for certain applications requiring long term surface stability.

In summary, pure titania experienced the anatase to rutile phase transformtion, followed by densification and grain growth. Pure rutile titaia was bioactive (but not highly), had a low strength and a low toughness. Zirconia addition into titania matrices tended to retard the densification, but once densified, the composites showed improved mechanical properties. For better mechanical properties and bioactivity, functionally gradient Y-TZP/Y-TZP-TiO_2/TiO_2-HA composites should be designed and fabricated in the future.

References

[1] M. Keshmiri, T. Troczymski, Apatite formation on TiO_2 anatase microspheres, J. Non-Cryst. Solids 324 (2003) 289-294.

[2] M. Uchida, H.M. Kim, T. Kokubo, S. Fujibayashi, T. Nakamura, Structural dependence of apatite formation on titania gels in a simulated body fluid, J. Biomed. Mater. Res. - Part A 64 (1) (2003) 164-170.

[3] M. Jokinen, M. Patsi, H. Rahiala, T. Pletola, M. Ritala, J.B. Rosenholm, Influence of sol and surface proerpteis on in vitro bioactivity of sol-gel derived TiO_2 and TiO_2-SiO_2 films deposited by dip-coating method, J. Biomed. Mater. Res. 42 (1998) 295-302.

[4] J.-M. Wu, S. Hayakawa, K. Tsuru, A. Osaka, Low-temperature preparation of anatase and rutile layers on titanium substrates and their ability to induce in vitro apatite deposition, J. Am. Ceram. Soc. 87 (9) (2004) 1635-1642.

[5] B. Fartash, H. Liao, J. Li, N. Fouda, L. Hermansson, Long-term evaluation of titania-based ceramics compared with commercially pure titanium in vivo, J. Mater. Sci. Mater. Med. 6 (1995) 451-454.

[6] S. Areva, H. Paldan, T. Peltola, T. Narhi, M. Jokinen, M. Linden, Use of sol-gel-derived titania coating for direct soft tissue attachment, J. Biomed.Mater. Res. - Part A 70 (2) (2004) 169-178.

[7] A.J. McManus, R.H. Doremus, R.W. Siegel, R. Bizios, Evaluation of cytocompatibility and bending modulus of nanoceramic/polymer composites, J. Biomed. Mater. Res. - Part A 72 (1) (2005) 98-106.

[8] K.S. Oh, F. Caroff, R. Famery, M.-F. Sigot-Luizard, P. Boch, Preparation of TCP-TiO_2 biocomposites and study of their cytocompatibility, J. Euro. Ceram. Soc. 18 (13) (1998) 1931-1937.

[9] J. Li, S. Forberg, L. Hermansson, Evaluation of the mechanical properties of hot isostatically pressed titania and titania-calcium phosphate composites, Biomaterials 12(4) (1991) 438-440.
[10] K. Hanada, T. Shoji, M. Mayuzumi, T. Sano, Development of self-lubricating titania/diamond nanoparticle composite, Materials Science and Technology 20 (9) (2004) 1103-1108.
[11] X. Miao, D. Sun, P.W. Hoo, J. Liu, Y. Hu, Y. Chen, Effect of titania addition on yttria-stabilised tetragonal zirconia ceramics sintered at high temperatures, Ceram. Int. 30(6) (2004) 1041-1047.
[12] C. Piconi, G. Maccauro, Zirconia as a ceramic biomaterial: a review, Biomaterials 20 (1999) 1-25.
[13] X. Ding, X. Liu, Synthesis and microstructure control of nanocrystalline titania powders via a sol-gel process, Mater. Sci. Eng. A224 (1997) 210-215.
[14] A.G. Evans, E.A. Charles, Fracture toughness determinations by indentation, J. Am. Ceram. Soc. 59 (1976) 371-372.
[15] T. Kokubo, H.-M. Kim, M. Kawashita, Novel bioactive materials with different mechanical properties, Biomaterials 24 (13) (2003) 2161-7215.
[16] L. Hao, J. Lawrence, K.S. Chian, D.K.Y. Low, G.C. Lim, H.Y. Zheng, The formation of a hydroxyl bond and the effects thereof on bone-like apatite formation on a magnesia partially stabilized zirconia (MgO-PSZ) bioceramic following CO/sub 2/ laser irradiation, J. Mater. Sci.: Mater. Med. 15 (9) (2004) 967-975.
[17] X.-B. Zhao, X.-Y. Liu, C.-X. Ding, Acid-induced bioactive titania surface, J. Biomed. Mater. Res. Part A 75A (4) (2005) 888 – 894.
[18] M. Uchida, H.-M. Kim, T. Kokubo, K. Tanaka, T. Nakamura, Structural dependence of apatite formation on zirconia gels in a simulated body fluid, J. Ceram. Soc. Jap. 110 (8) (2002) 710-715.
[19] M. Uchida, H.M. Kim, F. Miyaji, T. Kokubo, T. Nakamura, Apatite formation on zirconium metal treated with aqueous NaOH, Biomaterials 23 (1) (2002) 313-317.
[20] M. Uchida, H.-M. Kim, T. Kokubo, M. Nawa, T. Asano, K. Tanaka, T. Nakamura, Apatite-forming ability of a zirconia/alumina nano-composite induced by chemical treatment, J. Biomed. Mater. Res. 60 (2) (2002) 277-282.

Figure Captions

Figure 1 SEM micrograph showing the large titania particles and the small Y-TZP particles of the titania-10vol% Y-TZP mixed powder.

Figure 2 TG/DTA curves of the pure titania-precursor powder at a heating rate of 10°C/min up to 1000°C.

Figure 3 Sintering shrinkage rates of the titania-Y-TZP compacts with different Y-TZP contents versus temperature when the samples were heated at the heating rate of 5°C/min.

Figure 4 XRD patterns of the titania-Y-TZP samples sintered at 1300°C for 4 hours: (a) pure titania, (b) titania-5vol%Y-TZP, (c) titania-10vol%Y-TZP, and (d) titania-15vol%Y-TZP.

Figure 5 SEM micrographs of titania-Y-TZP samples sintered at 1200°C for 4 hours: (a) pure titania and (b) titania-15vol%Y-TZP composite.

Figure 6 SEM micrographs of the titania-Y-TZP samples sintered at 1350°C for 4 hours: (a) pure titania and (b) titania-15vol% Y-TZP composite.

Figure 7 Relative densities of the titania-Y-TZP composites sintered at different temperatures as a function of the Y-TZP content.

Figure 8 Titania grain size in the titania-Y-TZP composites sintered at different temperatures as a function of the Y-TZP content.

Figure 9 Hardness of the titania-Y-TZP composites sintered at different temperatures as a function of the Y-TZP content.

Figure 10 Flexural strength of the titania-Y-TZP composites as a function of the Y-TZP content.

Figure 11 Fracture toughness of the titania-Y-TZP composites as a function of the Y-TZP content.

Figure 12 SEM micrographs showing the surfaces of titania-15vol%Y-TZP composite subjected to (a) 5M HCl treatment and 20 day immersion in the SBF, and (b) 5M HCl treatment and 30 day immersion in the SBF.

Table

Table 1 Effect of surface treatment and the time of immersion in the SBF on the formation of apatite layer.

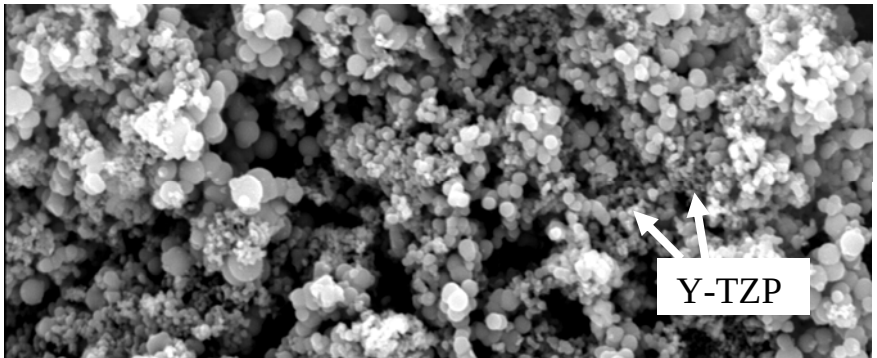

Figure 1 SEM micrograph showing the large titania particles and the small Y-TZP particles of the titania-10vol% Y-TZP mixed powder.

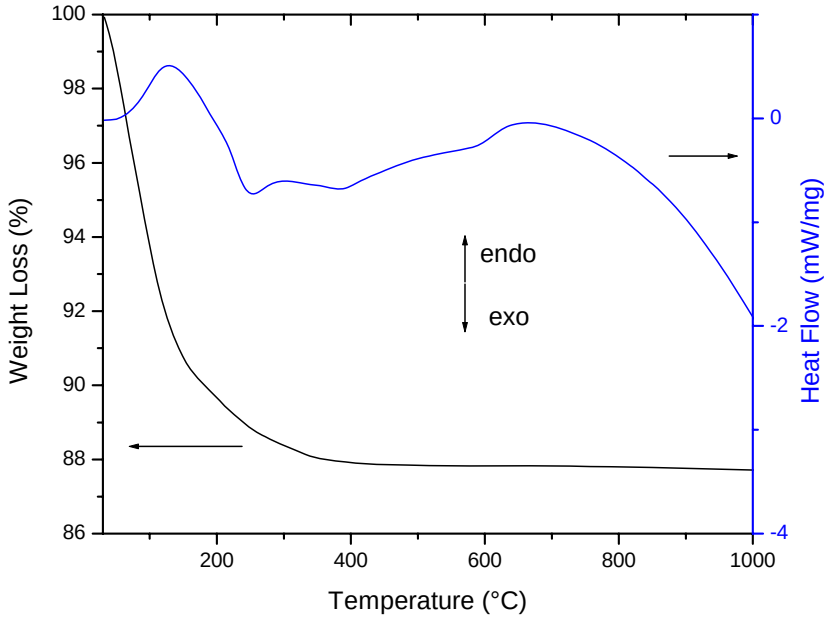

Figure 2 TG/DTA curves of the pure titania-precursor powder at a heating rate of 10°C/min up to 1000°C.

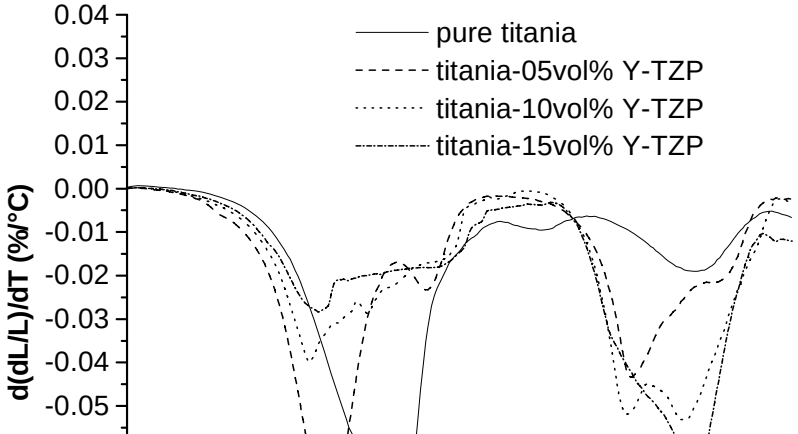

Figure 3 Sintering shrinkage rates of the titania-Y-TZP compacts with different Y-TZP contents versus temperature when the samples were heated at the heating rate of 5°C/min.

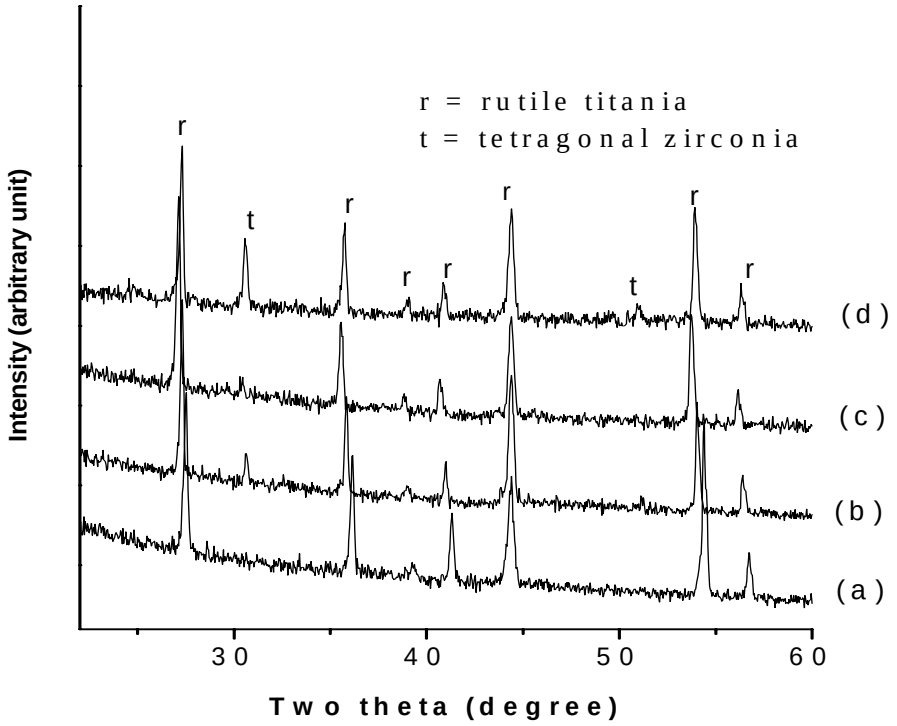

Figure 4 XRD patterns of the titania-Y-TZP samples sintered at 1300°C for 4 hours: (a) pure titania, (b) titania-5vol%Y-TZP, (c) titania-10vol%Y-TZP, and (d) titania-15vol%Y-TZP.

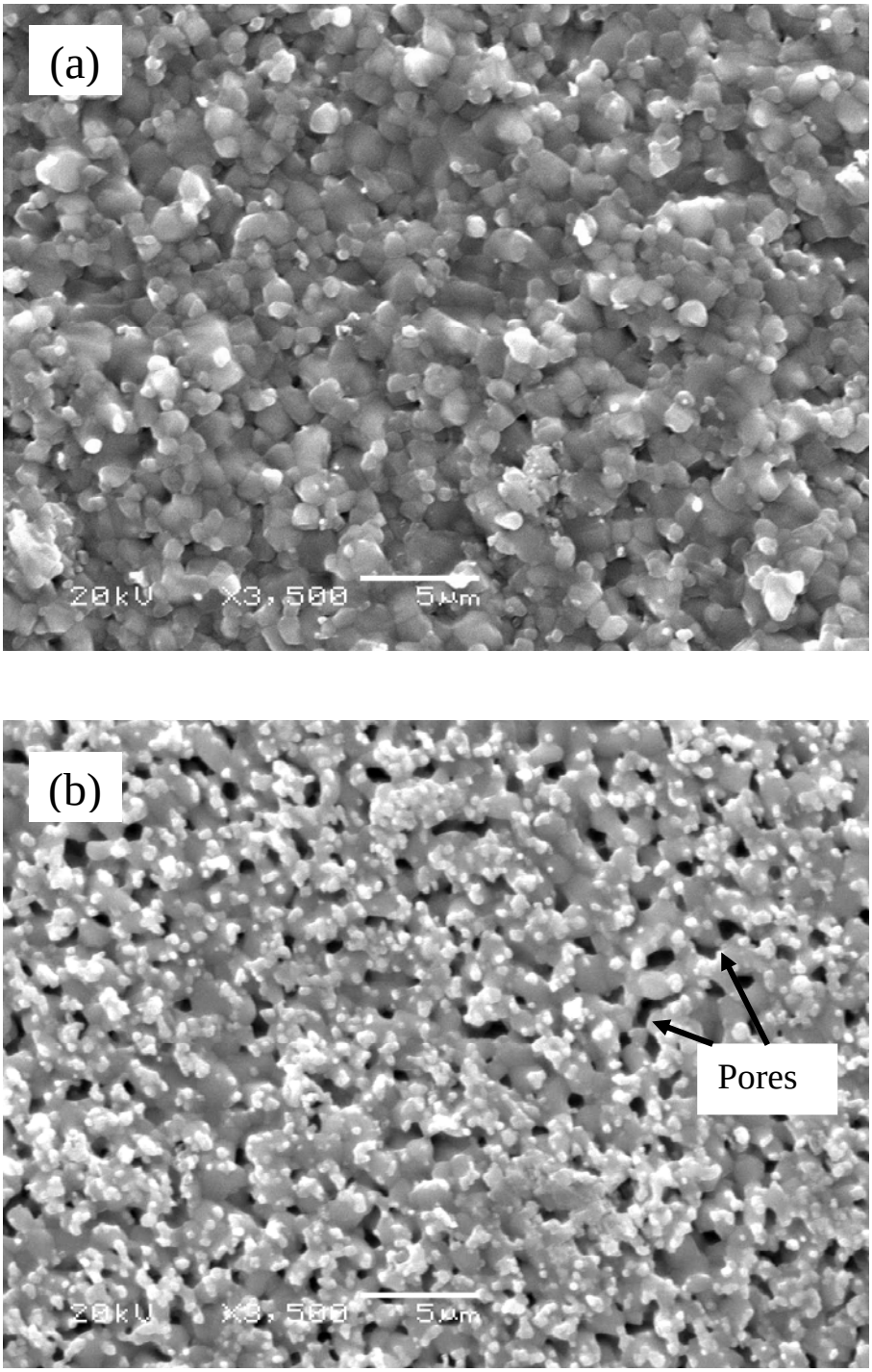

Figure 5 SEM micrographs of titania-Y-TZP samples sintered at 1200°C for 4 hours: (a) pure titania and (b) titania-15vol%Y-TZP composite.

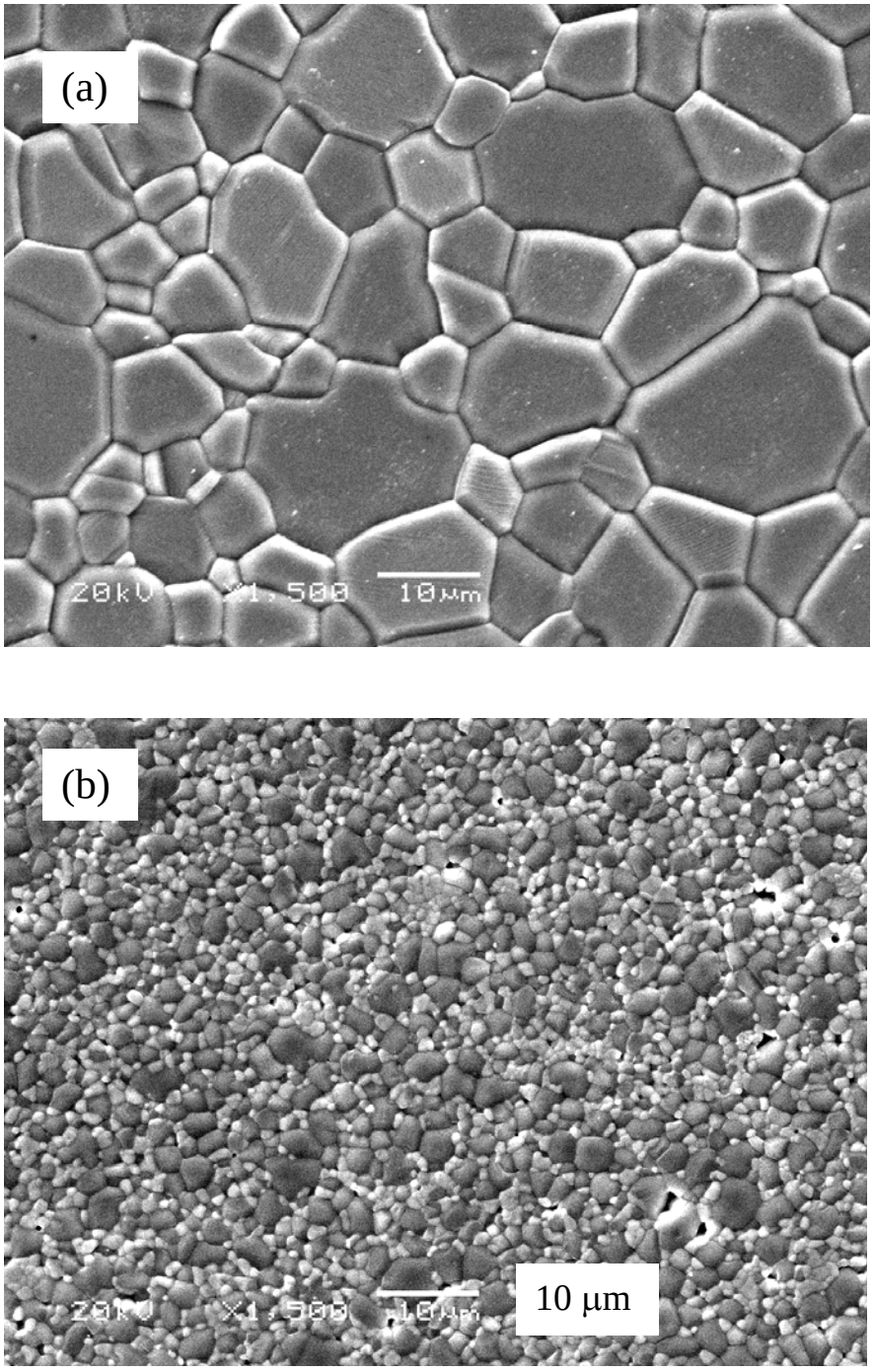

Figure 6 SEM micrographs of the titania-Y-TZP samples sintered at 1350°C for 4 hours: (a) pure titania and (b) titania-15vol% Y-TZP composite.

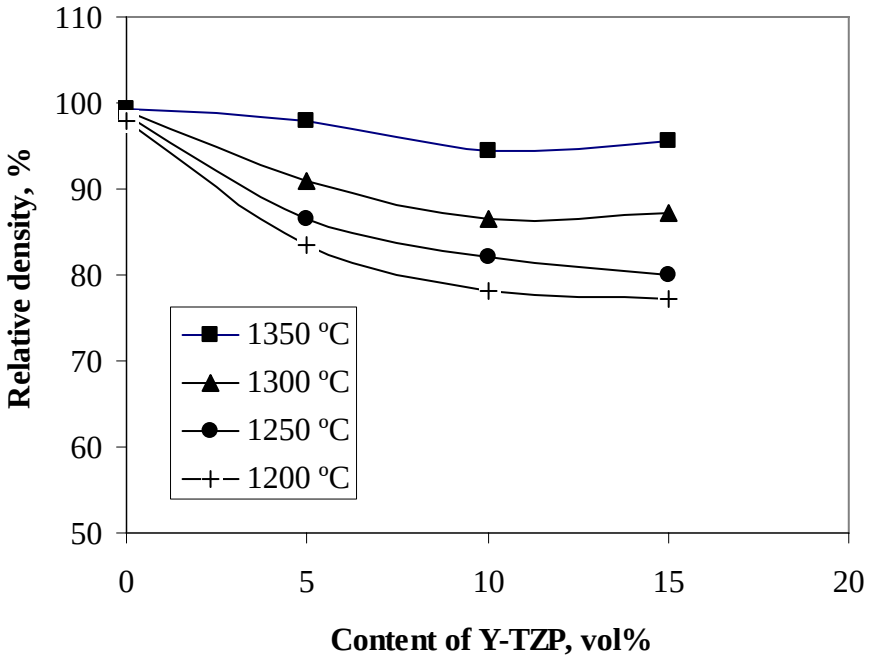

Figure 7 Relative densities of the titania-Y-TZP composites sintered at different temperatures as a function of the Y-TZP content.

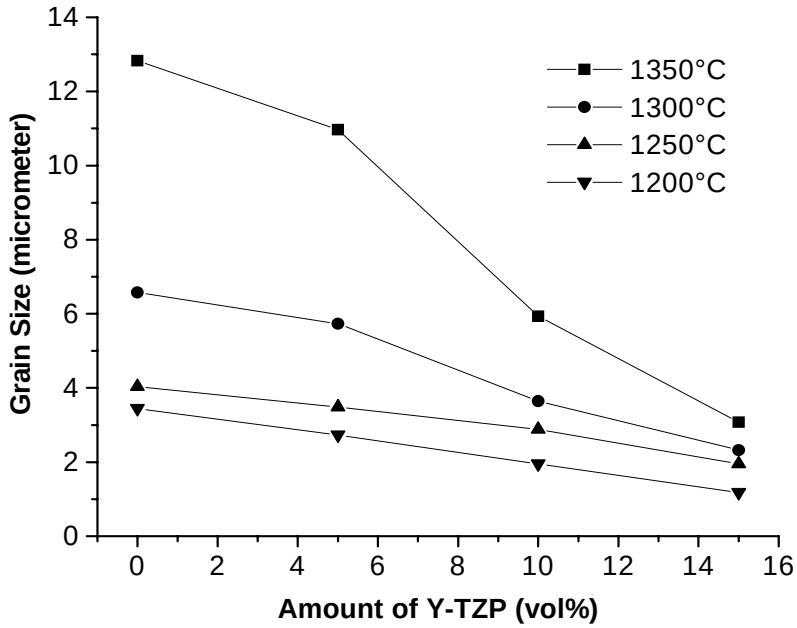

Figure 8 Titania grain size in the titania-Y-TZP composites sintered at different temperatures as a function of the Y-TZP content.

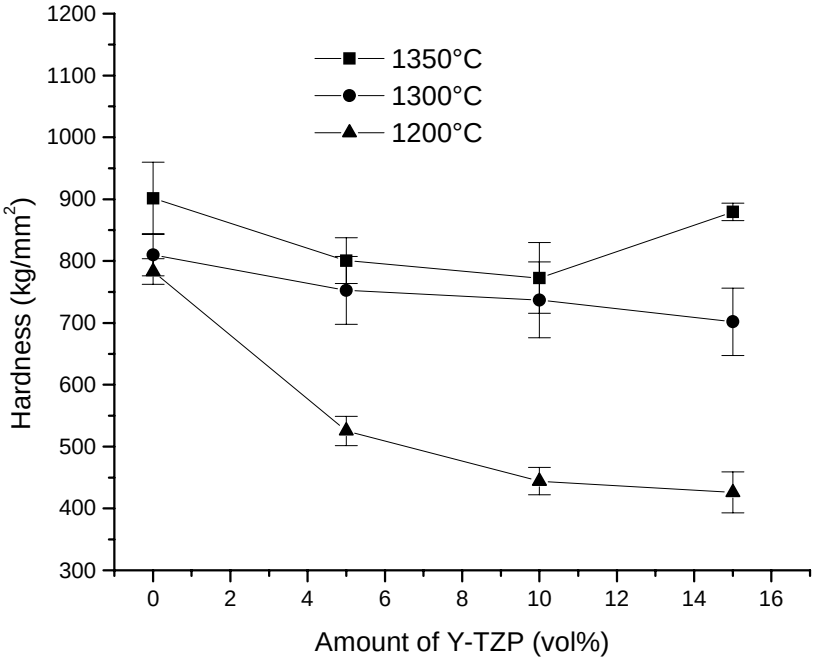

Figure 9 Hardness of the titania-Y-TZP composites sintered at different temperatures as a function of the Y-TZP content.

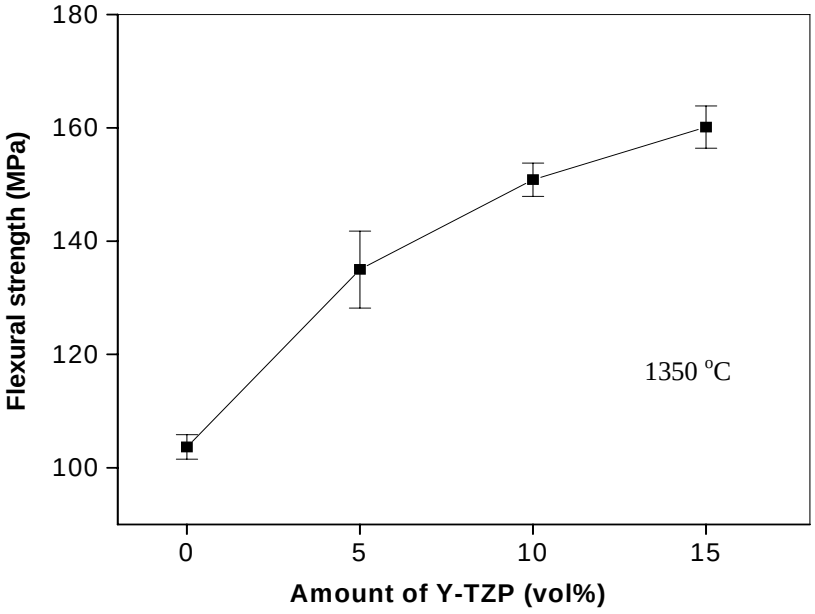

Figure 10 Flexural strength of the titania-Y-TZP composites as a function of the Y-TZP content.

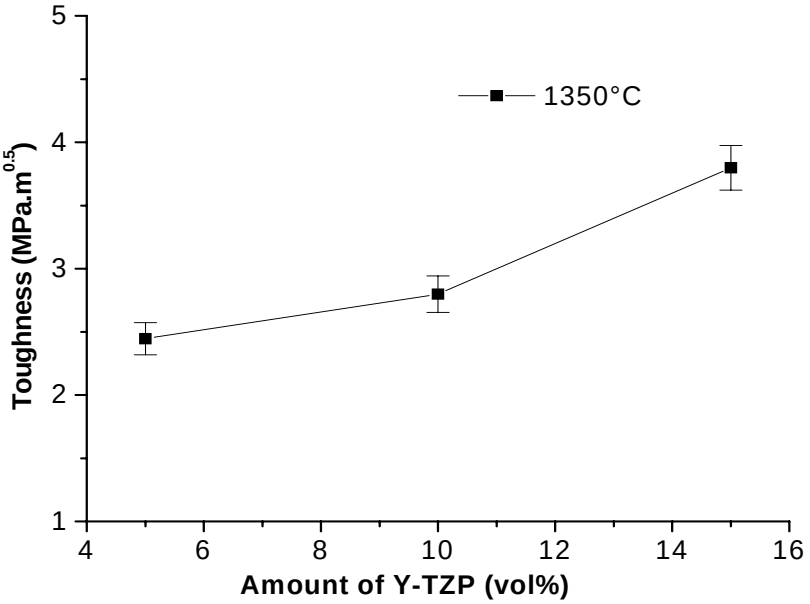

Figure 11 Fracture toughness of the titania-Y-TZP composites as a function of the Y-TZP content.

Table 1 Effect of surface treatment and the time of immersion in the SBF on the formation of apatite layer.

Samples	Treatment	7 Days	20 Days	30 Days
Pure titania	As-polished	No apatite	Islands of apatite	Apatite layer
Titania-15vol% Y-TZP	As-polished	No apatite	No apatite	No apatite
Titania-15vol% Y-TZP	5M HCl	No apatite	Islands of apatite	Apatite layer

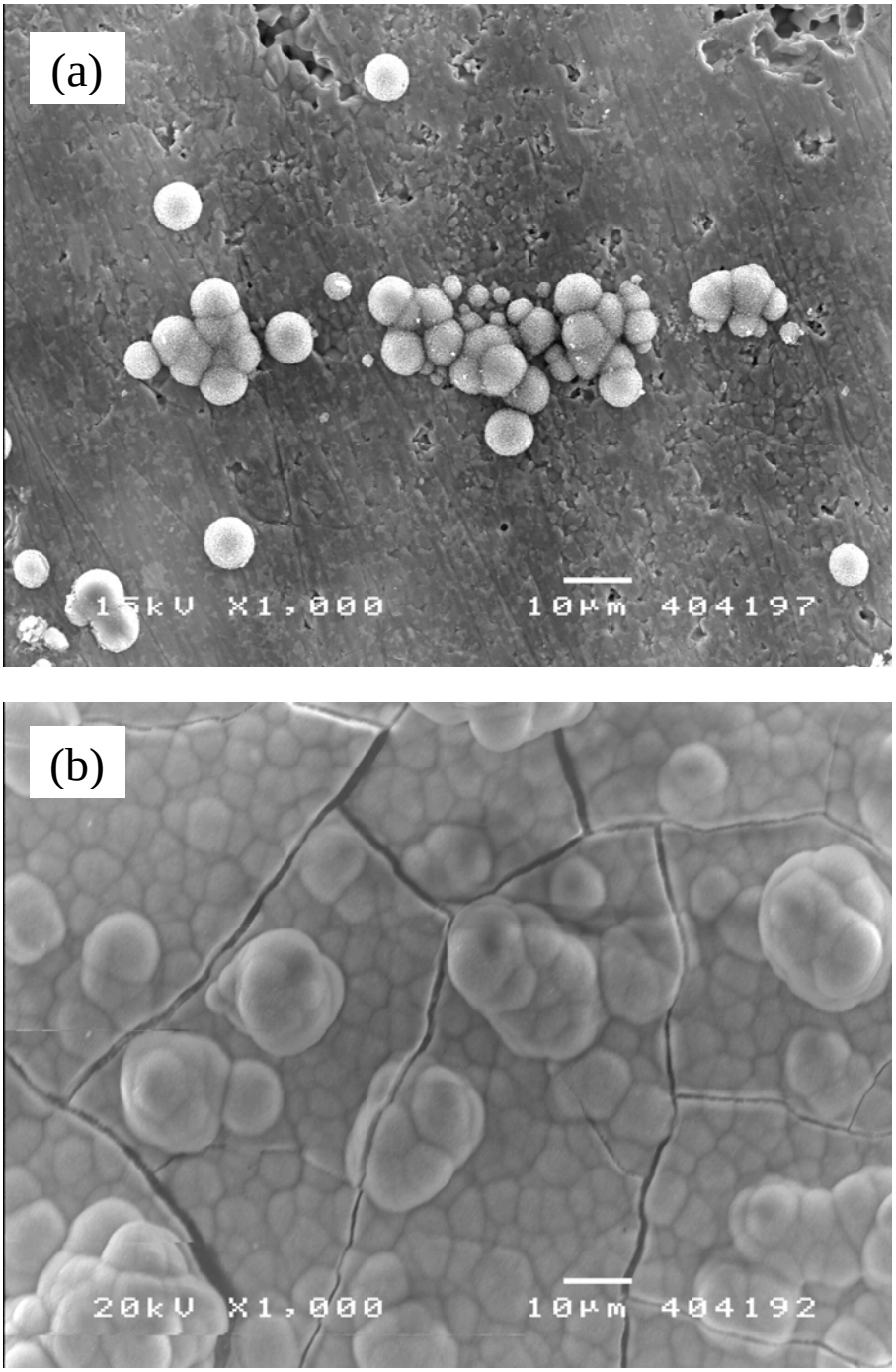

Figure 12 SEM micrographs showing the surfaces of titania-15vol%Y-TZP composite subjected to (a) 5M HCl treatment and 20 day immersion in the SBF, and (b) 5M HCl treatment and 30 day immersion in the SBF.